A Dual 3-Element Nulling Interferometer for TPF

T.Velusamy, C.A Beichman, M. Shao

Jet Propulsion Laboratory, California Institute of Technology, Pasadena, CA 91109

Abstract. We present an interferometer design that provides a null at the star and a direct measurement of both visibility amplitude and phase of the planets. Six telescopes are configured to form two identical nulling interferometers. Each nulling interferometer with 3 telescopes, aperture sizes (1:2:1) on a baseline 30- 50 m, produces a θ^4 null. They are placed on a longer baseline ($\sim$ 100- 1000 m). The null beams are combined to produce a chopped output, by introducing a phase shift in one of the beams, and by switching it between 0° and 180° (cosine chop) or between 90° and 270° (sine chop). The sine/cos chops measure directly the complex visibility of the planets. Simple synthesis techniques are used for image reconstruction by measuring the visibilities in a number of u-v points by rotating the baselines. This scheme has an enhanced capability for planet detection and characterization.

1. Introduction

The primary goal of Terrestrial Planet Finder (TPF) is direct detection of emission from extra-solar Earth-like planets and to characterize its habitable nature using infrared spectroscopy at 7 - 20 μm. Some of the designs under investigation are described in the TPF book edited by Beichman et al (1999). Several improvements to the original concept of nulling pupil plane interferometry (Bracewell & McPhie 1979) have been suggested (e.g. 4-element linear array by Angel & Wolf (1997); 2-D arrays by Leger et al 1996). These interferometers provide only a measure of the fringe amplitude of the planet and a cross-correlation analysis is used for image reconstruction. These images have a 180° ambiguity in planet's position angle (this can be removed by chopping with a phase shift as shown by Shao 1996). Simulations have shown that these configurations have limitations for planet detection when exo-zodi > 1Z and at inclinations > 30° (Beichman & Velusamy 1999). Arrays in which the individual elements themselves are nulling interferometers have been suggested by Shao (1996) and Woolf & Angel (1997) which provide both nulling and chopping. Here we discuss a six telescope nulling interferometer which measures both amplitude and phase of the visibility.

2. Dual 3-element nulling interferometer

Figure 1 shows schematic sketch of the 6-telescope TPF. The basic design is that of a phase shifting two element interferometer which measures both the sine and

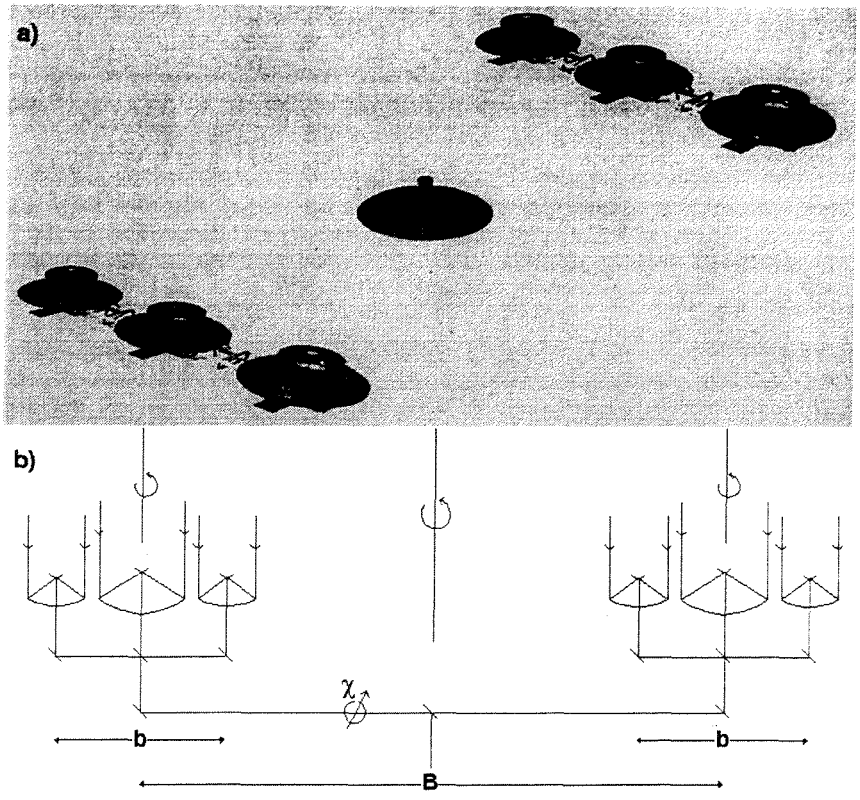

Figure 1. (a) An artist sketch of 6-telescope TPF. (b) A schematic of the nulling interferometers and the combiner for the nulled beams. A chopped output is obtained by switching a variable phase shift χ in one of the nulled beams.

cosine fringe amplitudes. Each element itself is a nulling interferometer which produces a nulled beam formed by combining 3 telescopes of sizes 1:2:1 in a linear array. The baseline of the nulling interferometer **b** is $\sim$ of 30-50m. The sine and cosine fringes on the planets are obtained with the longer (imaging) baseline **B** $\sim$ 100- 1000 m, between the nulling elements. The nulling interferometers can be flown on two separate free flyers and the chopper & beam combiner on a third free flyer as indicated in Figure 1a. Because the nulling and imaging baselines are independent, the characteristics of the null response (determined by **b**) and spatial resolution (determined by **B**) are totally de-coupled. This is a big advantage because in other configurations, increasing the baseline to achieve higher spatial resolution would lead to a narrower null which will result in resolving the central star.

3. Interferometry with Nulled Beams

The response of a 3-element nulling interferomter (1:2:1) is

$$P_{null} \sim sin^4\phi/2 \tag{1}$$

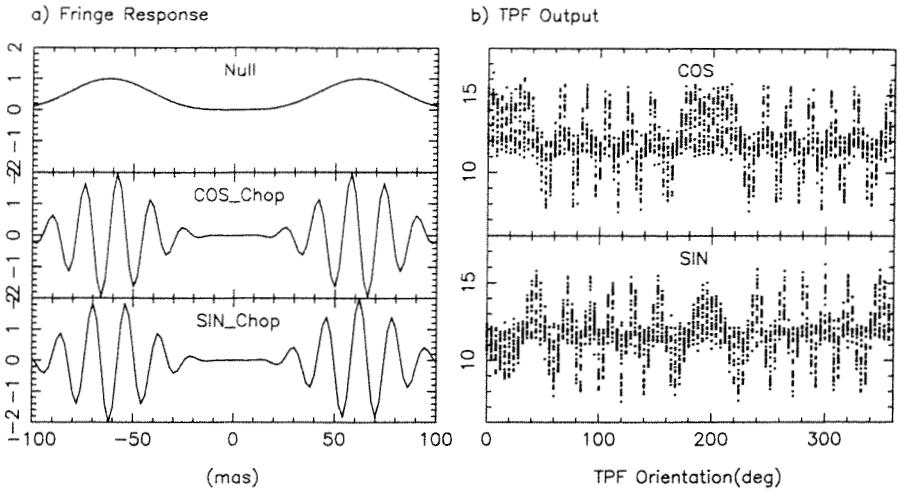

Figure 2. (a) The null, sine and cosine chop responses. (b) Sine/cosine chop outputs as a function of the orientation of the imaging baseline **B** between the nulling interferometers. The amplitude spread in the outputs at each orientation is due to the rotation of the null baseline. The complex visibility at each orientation (corresponding to one u-v sample) are determined from the mean amplitude of the sine and cosine chop outputs. $\lambda = 12$ μm and baselines b=40m, B=150m.

where $\phi = \pi \mathbf{b}.\mathbf{S}/\lambda = \pi(b/\lambda)\theta Cos(\beta - \alpha)$, (α, θ) off axis sky position, and β is position angle of the baseline. The width of the null response $\sim$ 3-4 mas for $< 10^{-6}$ at 12μm and has an off axis null $\sim \theta^4$. The response of the interferometer formed by the nulled beams with a phase shift χ in one of the null beams,

$$I_{out}(\chi) = P_{null}[1 + cos(\Phi - \chi)] \tag{2}$$

where, $\Phi = 2\pi \mathbf{B}.\mathbf{S}/\lambda = 2\pi(B/\lambda)\theta Cos(\gamma - \alpha)$, where (α, θ) is the off axis sky position, and γ is position angle of the baseline **B**. The chopped output response,

$$I_{Cos-chop} = I_{out}(\chi = 0) - I_{out}(\chi = \pi) = 2P_{null} cos\Phi \tag{3}$$

$$I_{Sin-chop} = I_{out}(\chi = \pi/2) - I_{out}(\chi = 3\pi/4) = 2P_{null} sin\Phi \tag{4}$$

When B >> b, $\Phi >> \phi$, the null response as function of θ (eq. 1) varies more slowly than the sinusoidal fringe term (in eq. 3 & 4). Thus the chopped output responses represent sine and cosine fringe pattern as a function of (x,y) or (θ, α) whose amplitude is modified by the slowly varying null response pattern. Figure 2a shows the interferometer responses in the sky along the x-axis, the baseline vector **B**. (When the nulling and imaging baselines are comparable, B $\sim$ b the response is no longer sinusoidal and reduces to a complex pattern as shown for example, by Woolf & Angel (1997)). Since,

$$\Phi = 2\pi \mathbf{B}.\mathbf{S}/\lambda = 2\pi(ux + vy) \tag{5}$$

the chopped outputs (eq 3 & 4) measure the real and imaginary quantities of the complex visibility at the u-v corresponding to **B**. Thus the observed complex

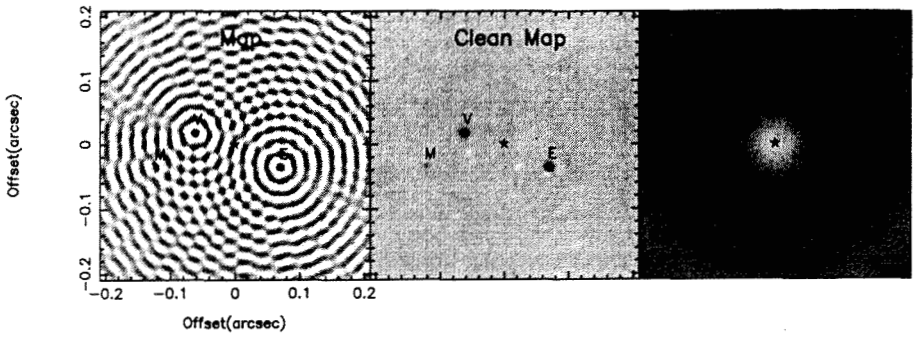

Figure 3. Imaging a solar system analog with Earth, Mars and Venus at 10 pc. $\lambda = 14$ μm and baselines b=30m , B=150m.

visibility,

$$V_{obs}(u,v) = \int_x \int_y P_{null}(x,y,\beta) I(x,y) e^{2\pi i(ux+vy)} dxdy \tag{6}$$

The integration in x,y is over the fov and $P_{null}(x,y,\beta)$ represents the the null response for baseline vector **b** at any orientation β. Eq. 6 allows us to reconstruct the image of the extra-solar planets by a simple Fourier transform of the observed visibilities. The observed intensity distribution is the true image attenuated by the null response,

$$I_{obs}(x,y) = P_{null}(x,y,\beta) I(x,y) \tag{7}$$

I(x,y) is obtained by correcting for the null response. The imaging baseline **B** is rotated to sample different u,v points while keeping the nulling baseline **b** fixed. But the planet could be located near a minimum in the null response. If planet position is known, null baseline (length and orientation) may be adjusted to bring the planet near a maximum in the null response. However this can be matched only for a given wavelength. The baselines of the nulling and imaging interferometers can be rotated independently. Rotating the null baseline through 0° to 180° enables that each planet is observed near the maximum in the null response at a few orientations for any wavelength. This allows a fairly uniform sensitivity for planet detection in the fov, for each u-v measurement. Figure 2b shows the outputs obtained by rotating both the baseline vectors **b** & **B**, plotted against the orientation of the imaging baseline. The spread in the amplitude at each orientation is the result of the rotation of the null baseline. By using the average values at each orientation, the Fourier transformed image,

$$I_{obs}(x,y) = \langle P_{null}(x,y) \rangle_\beta I(x,y) \tag{8}$$

Figure 3 shows an example of this approach for imaging a solar system analog with Mars, Venus and Earth at a distance of 10 pc. To obtain the true flux of the planets the intensities in the clean map are corrected for the average null response, $\langle P_{null}(x,y) \rangle_\beta$.

4. Planet Detection and Characterization

Direct imaging of extra-solar Earth-like planets requires, in addition to the nulling of the central star, high fidelity imaging capable of detecting a weakly enhanced planet emission against a bright exo-zodi in which the planets are embedded. Planet detection alone can be relatively easy because the u-v data at all wavelengths can be combined to produce a single image. But, the characterization of the planet by its spectrum in the 7 to 20 μm region requires a capability for accurate measurements of planet flux density at each wavelength.

4.1. Map Fidelity

The main source factors that affect the fidelity of the image are the exo-zodi strength, inclination of the local ecliptic with respect to the line of sight, and structures in exo-zodi. The u-v coverage (number of baselines) and spatial resolution (length of baselines) are critical factors for map fidelity. Especially the complexity of the planetary system (i.e. if several planets are present) will require a good u-v coverage. The accuracy of the planet flux measurement will also depend on the degree of uniformity of the null response across the fov (see Fig. 3). The leakage of the star light through the null and the exo-zodi emission are the main sources of the photon noise in the outputs. The spectral study requires a uniform sensitivity at all wavelengths. But, several factors such as, the null width, spatial resolution, exo-zodi flux are wavelength dependent and affect differentially the image quality and sensitivity at different wavelengths.

4.2. Simulation

In order to investigate the usefulness of the imaging technique described above, we present here the results of our simulations. We assumed a solar type star at a distance of 10 pc observed with a dual 3-element interferometer at 1 AU orbit. A detailed analysis of the exo-zodi emission and the signal to noise are discussed by Beichman & Velusamy (1999). A randomly fluctuating component on the scale $\sim$ 0.1 AU at 0.5% level, and a 0.1 AU wide band emission with 1 AU radius at 10% level were added onto a smooth exo-zodi emission. The strength of the zodi was varied from 1 to 20 Z. Several inclinations of the ecliptic of the extra-solar planetary systems were also studied. Telescope aperture sizes of 3.5 m and 1.75 m were assumed. The pointing jitter was 0.25 mas. An integration time of 10^5 sec was assumed for one set of baselines (b, B) and their rotation.

Figure 4 shows some examples of the images obtained by simulations. In the case of solar system analog with 1Z, all three planets Mars, Venus and Earth are easily detected in a single wavelength map for inclinations of the ecliptic $<$ 75°, at still higher inclinations only Earth and Venus are detectable. This result is a very significant improvement over the other configurations in which the large axial ratio in the exo-zodi for high inclinations, introduces a large modulation in their output with rotation of the baseline. This effect is significantly reduced in the present configuration because of the sinusoidal fringe response of the interferometer (Fig. 2a). As demonstrated in Figure 5, a moderate single baseline of $\sim$ 150 m provides the fidelity required to study the spectral characteristics of the planet. However, longer baselines $\geq$ 300 m are required to detect Earth-like planets in the case of strong exo-zodi $\sim$ 10Z (see Figure 4b).

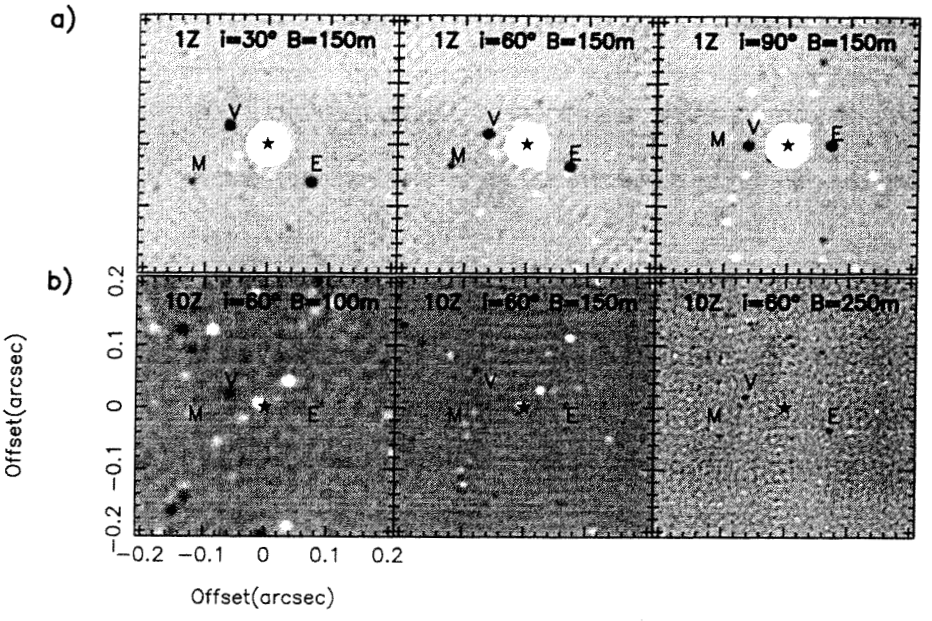

Figure 4. Imaging a solar system analog with 3 planets at $\lambda = 14$ μm. (a) Exo-zodi strength 1Z at inclinations of the ecliptic as marked. Baselines b=30m , B=150m. (b) Effect of baseline on the image fidelity. Exo-zodi strength 10Z at inclination 60°. Baselines b=30 m and B as marked. Note Earth and Venus are detectable only for B > 200 m.

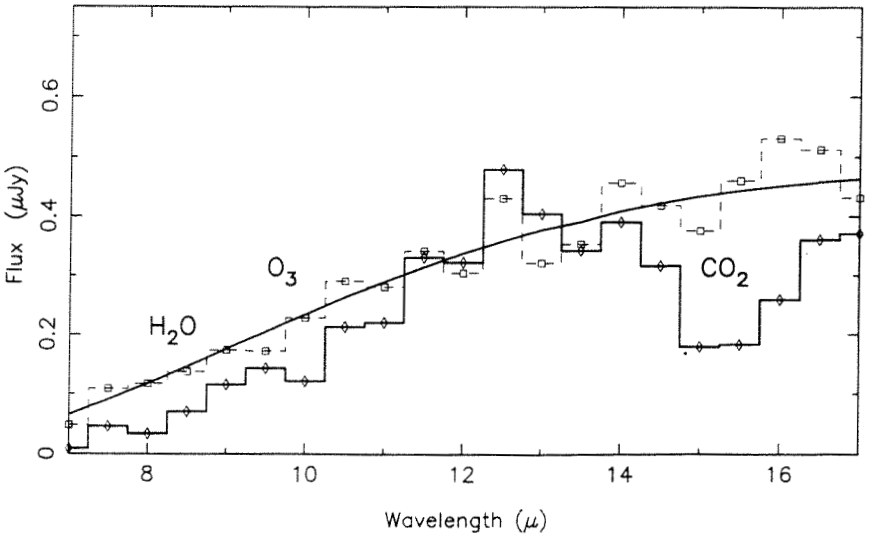

Figure 5. Spectrum of the Earth as obtained from the simulated images. The solid line represents the black body spectrum. The points represent the flux densities observed in the simulation for Earth with atmosphere (◇) and without atmosphere (□).

5. Conclusion

Combined with the nulling and all the features of synthesis imaging, the dual 3-element interferometer has great potential for detecting and characterizing Earth-like planets in extra-solar planetary systems. Its nulling and chopping features has several advantages over the other configurations: Measures both amplitude and phase of the planet visibility, providing a straight forward synthesis imaging; the null width is independent of the spatial resolution, hence there is no restriction on the maximum baseline; the chopping reduces the exozodi emission and the longer baselines which are now possible resolve out the exo-zodi; chopping also alleviates the effects of any low frequency drifts in the null stability. Finally it has a great potential for general astrophysical imaging.

Acknowledgments. This research was conducted at the Jet Propulsion Laboratory, California Institute of Technology, under contract with NASA.

References

Angel, J.R.P. & Woolf, N.J. 1997, ApJ 475, 373

Beichman, C.A. & Velusamy, T. 1999 (in preparation)

Bracewell, R.N & McPhie, R.H. 1979, *Icarus* 38, 136

Lager et al. 1996, *Icarus* 123, 249

Shao, M. 1996, in Ex-NPS report

Woolf, N.J. & Angel, J.R.P. 1997, in *Planets beyond the solar system and the next generation of space missions* ASP Conference Series, ed. David Soderblom, p285